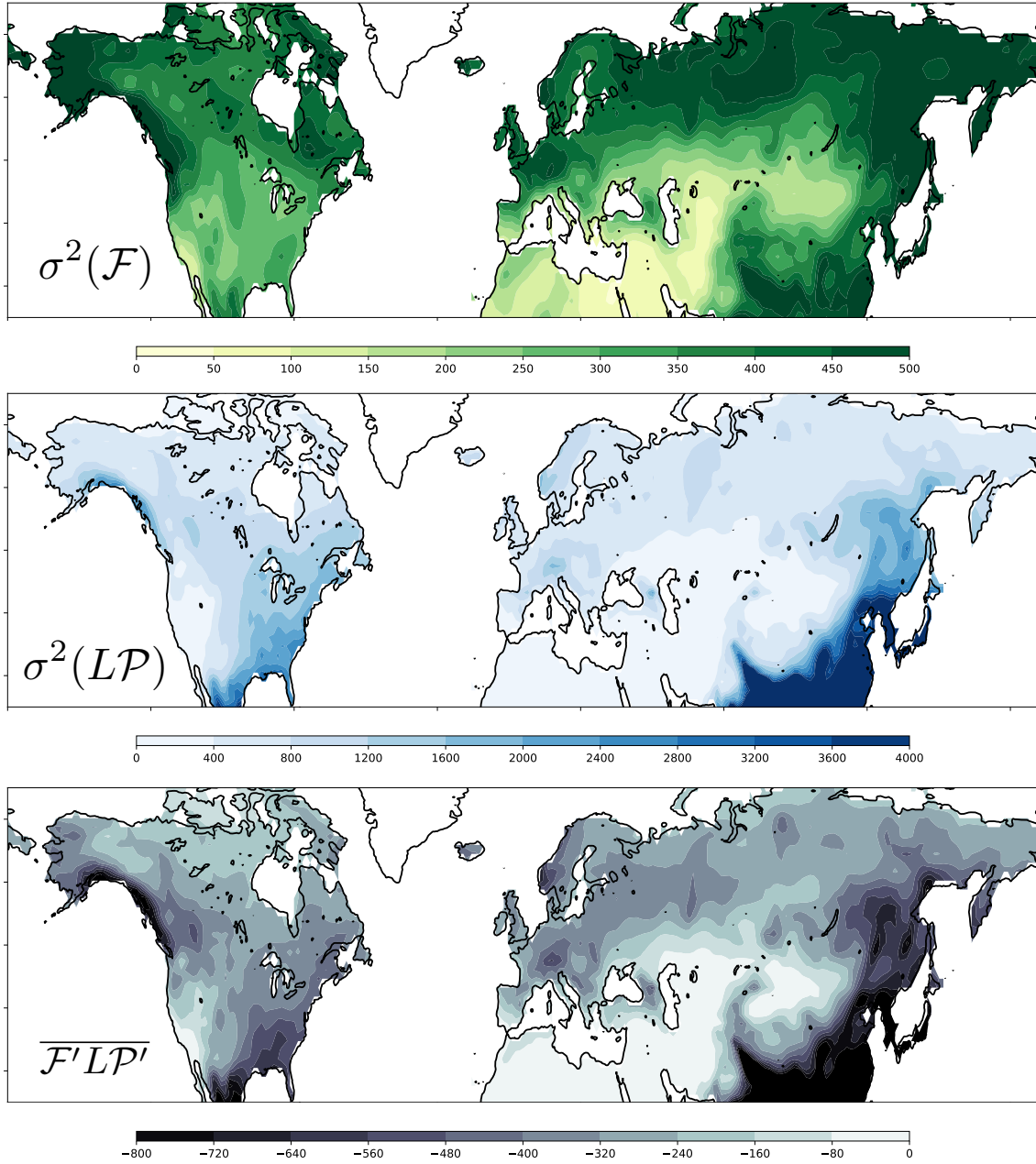Supporting Information for

Projected Increases in Summertime Temperature Variance are Driven by Local Thermodynamics

L.R. Vargas Zeppetello, D.S. Battisti
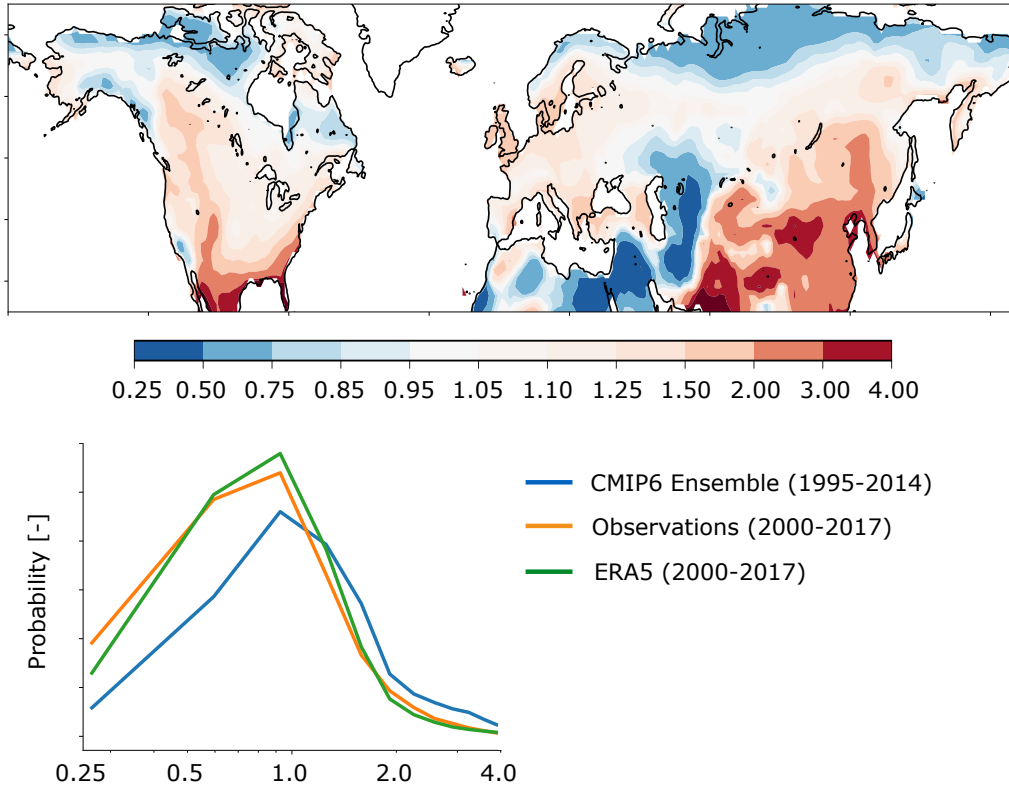
University of Washington Department of Atmospheric Sciences

Contents of this file

Figure S1: Forcing components used in Eq. 1. All terms given in W^2m^{-4}.
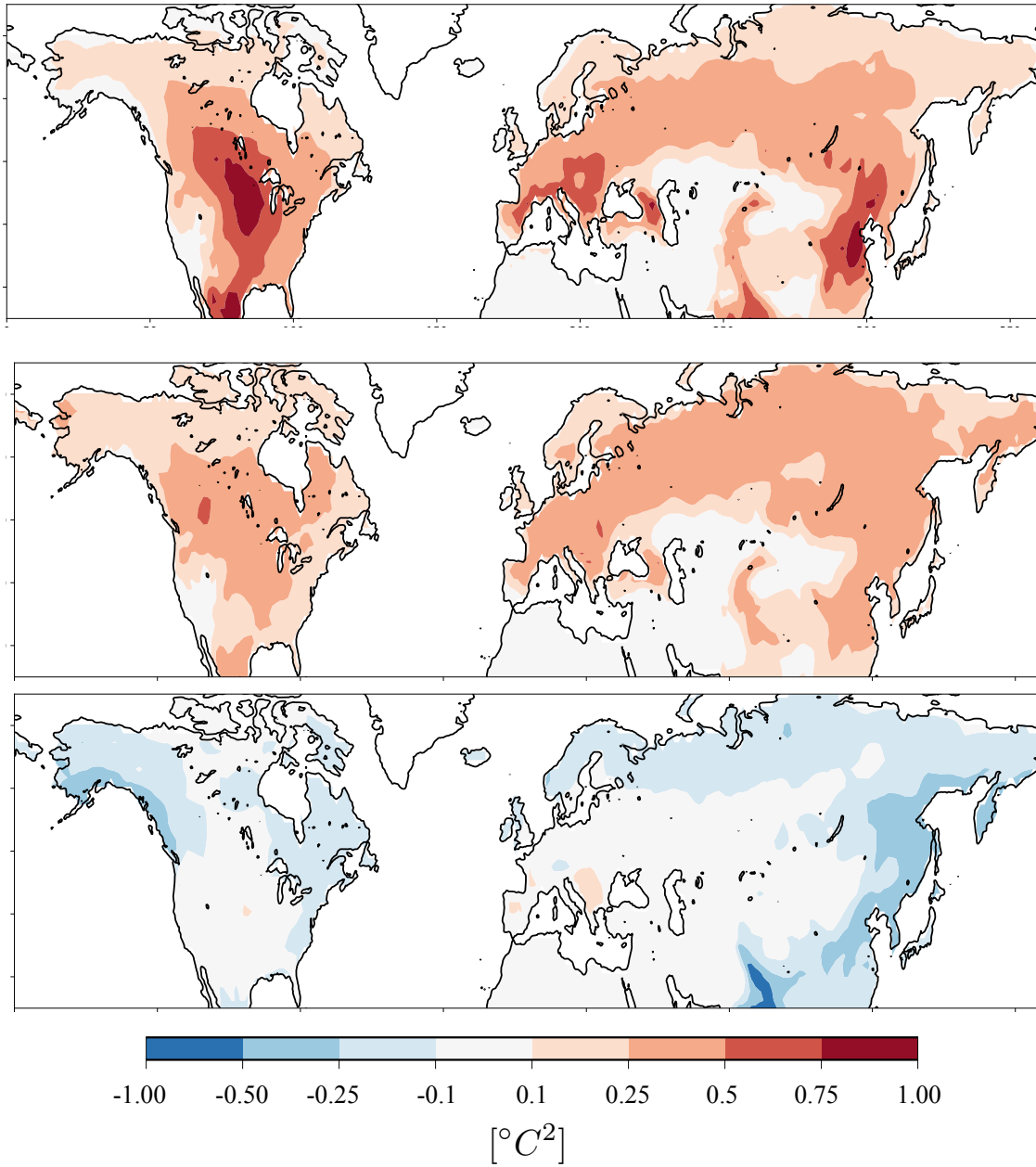
Figure S2: Top panel shows the ratio of temperature variance predicted by Eq. 1 using the forcing components from the CMIP6 ensemble (see Fig. S1) to the temperature variance in the CMIP6 ensemble for the last 20 years of the historical simulations. Bottom panel shows the probability distribution of this variance ratio north of 25°N for the CMIP6 ensemble (blue), and the variance ratio evaluating the diagnostic equation's accuracy in two other datasets (Observations and ERA5 reanalysis) analyzed in Vargas Zeppetello et al. (in press).

Importantly, while all three realizations of the diagnostic equations use different forcing values and aim to reproduce dataset-specific patterns of temperature variance, all use the same three parameter values for i) dry surface temperature sensitivity (v), ii) surface resistance (r_s), and iii) soil moisture sensitivity (μ).
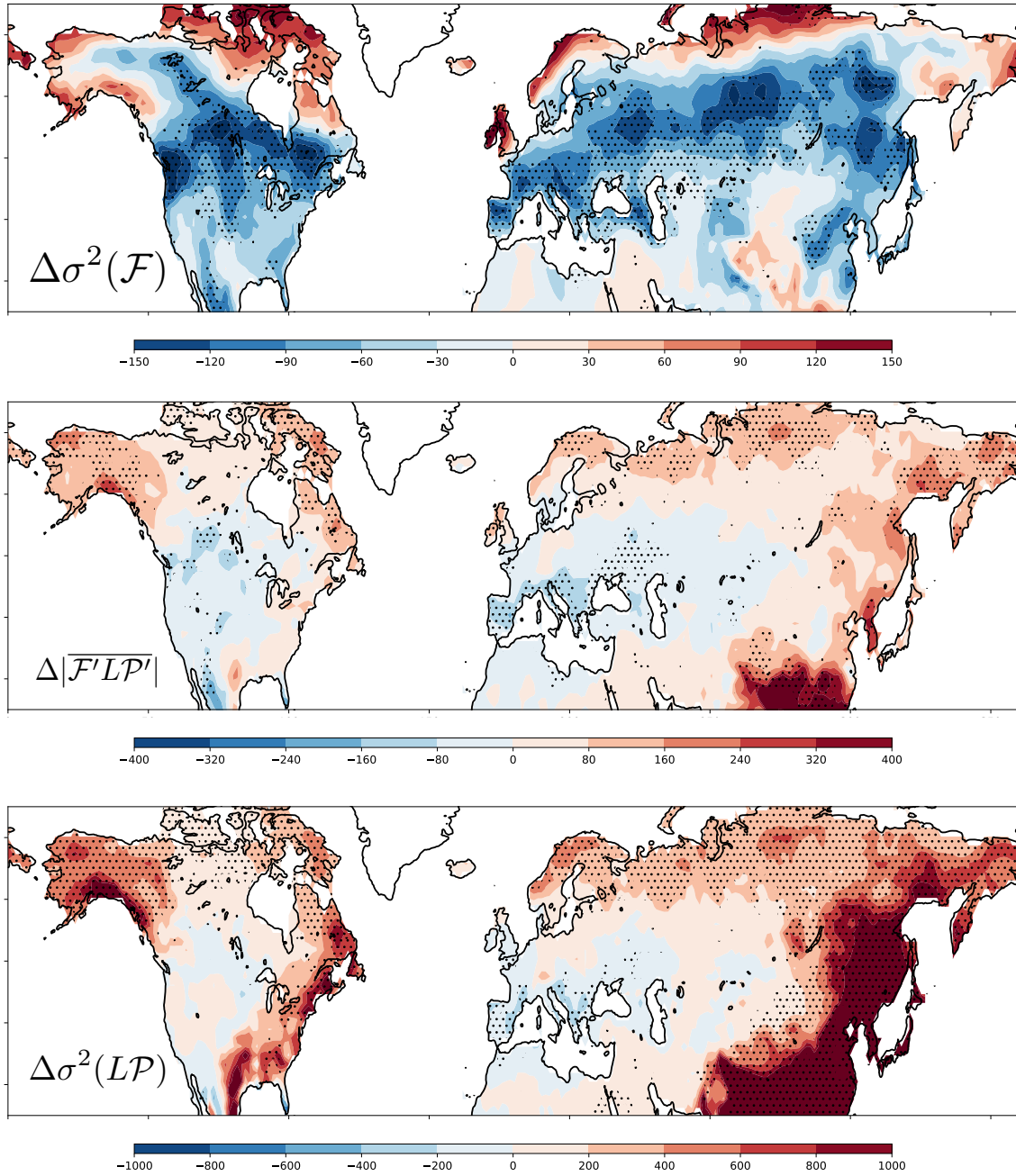
Figure S3: Changes in the forcing components between the end of the SSP585 scenario (2080-2099) and the end of the historical period (1995-2014). All values listed in W^2m^{-4}; dots show the grid cells where more than 75% of the models in the ensemble agree on the sign of the change. Note that the colorbars are different for each plot.

Figure S4: Changes in temperature variance associated with each term in Eq. 2. The top panel shows temperature variance changes associated with amplification of precipitation forcing (first term in Eq. 2), the middle panel shows the changes associated with amplification of the covariance forcing component (second term in Eq. 2), and the bottom panel shows the changes associated with the amplification of the base state temperature variance (third term in Eq. 2).
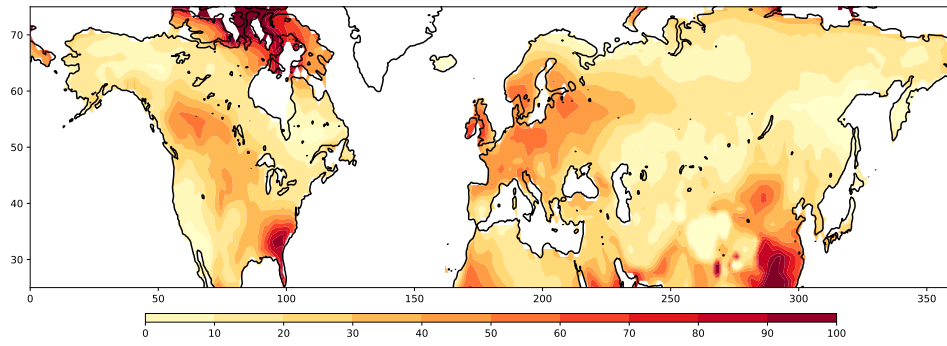
Figure S5: CMIP6 MMM temperature variance change between the end of SSP585 and the end of the historical period shown as a percentage departure from the historical period.

$$\Delta\sigma^2(T)_{MMM}$$

a)

$$\Delta\sigma^2(T)_{Diag}$$

b)

$$[°C^2]$$
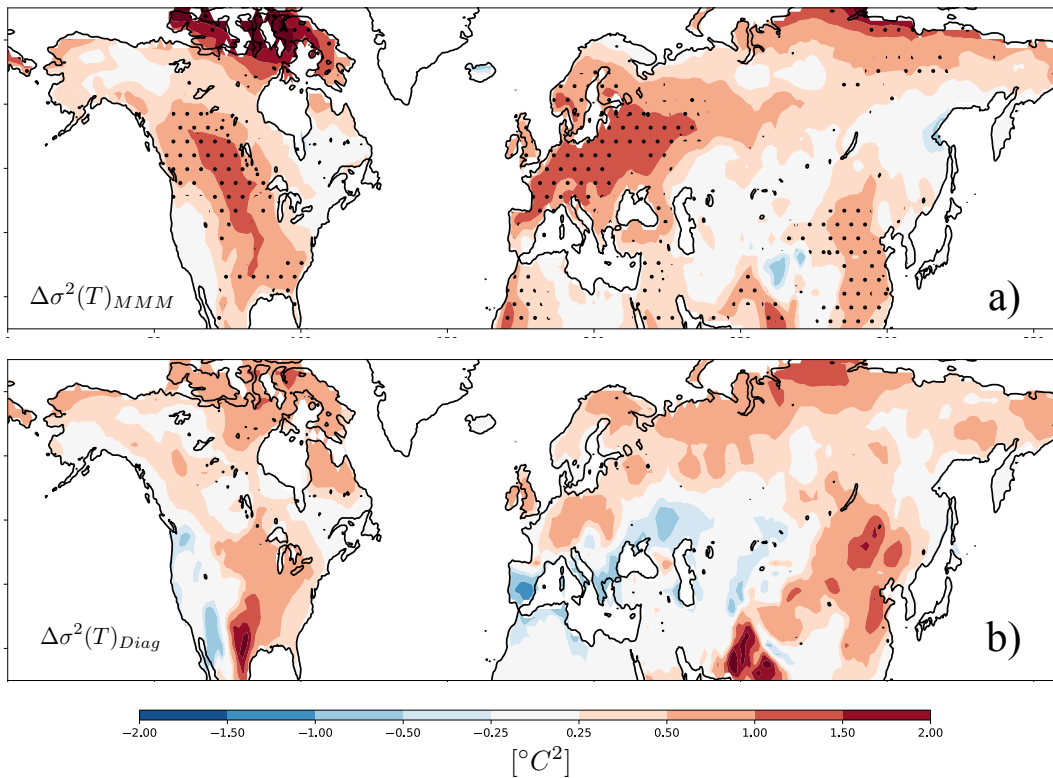
Figure S6: Panel a) is a reproduction of Fig. 2a from the main paper showing the change in temperature variance in the CMIP6 multi-model-mean between the end of the SSP585 scenario and the end of the historical simulations. Panel b) shows the temperature variance change predicted by the diagnostic model taking into account the forcing changes shown in Fig. S3 as well as the summertime warming and relative humidity changes. The agreement is slightly worse than the purely thermodynamic prediction shown in the main paper, for an explanation, see comment above.

Comment on Fig. S6:

The partial derivative taken in Eq. 2 gives the change in temperature variance due only to local warming. Other drivers of temperature variance certainly exist, and additional sensitivity tests of this diagnostic model are shown in Vargas Zeppetello et al. (2020). Figure S6b shows the temperature variance change calculated by subtracting two realizations of Eq. 1 with different values for the forcing components and local summertime mean state variables. We find that the approach presented in the main paper agrees more accurately with the CMIP6 multi-model-mean. This suggests that changes in environmental parameters used in the model or large scale changes in the underlying soil moisture distribution compensate for the changes in the forcing components shown in Fig. S3. These model parameters cannot be estimated from the standard model output and were therefore not considered in our study. However the differences between Figs. S6a, S6b, and 2b indicate that changes in the forcing components, environmental parameters, and underlying soil moisture distribution are of second order importance to the changes associated with local warming outlined in the main paper.

References:

Vargas Zeppetello, L.R., D.S. Battisti, M.B. Baker, 2020. "A New Look at the Variance of Summertime Temperatures Over Land" *J. Climate* 33(13) 5465-5477 doi: 10.1175/JCLI-D-19-0887.1

Model Name	Institution	Model Name	Institution
ACCESS-CM2	Commonwealth Scientific and Industrial Research Organization (Australia)	GISS-E2-1-G-CC	Ibid.
ACCESS-ESM1-5	Ibid.	GISS-E2-1-H	Ibid.
AWI-CM-1-1-MR	Max Planck Institute (Germany)	**HadGEM3-GC31-LL**	Hadley Centre for Climate Prediction and Research (U.K.)
BCC-CSM2-MR	Beijing Climate Center	HadGEM3-GC31-MM	Ibid.
CAMS-CSM1-0	Chinese Academy of Meteorological Sciences	**INM-CM4-8**	Institute for Numerical Mathematics (Russia)
CanESM5	Environment and Climate Change Canada	**INM-CM5-0**	
CESM2	National Center for Atmospheric Research (U.S.A.)	**IPSL-CM6A-LR**	**Institut Pierre Simon Laplace (France)**
CESM2-WACCM	Ibid.	MCM-UA-1-0	University of Arizona
CNRM-CM6-1	National Centre for Meteorological Research (France)	**MIROC6**	Japan Agency for Marine-Earth Science and Technology
CNRM-CM6-1-HR	Ibid.	**MIROC-ES2L**	Ibid.
CNRM-ESM2-1	Ibid.	MPI-ESM-1-2-HAM	Max Planck Institute (Germany)
E3SM-1-1	Department of Energy (U.S.A.)	**MPI-ESM1-2-HR**	Ibid.
E3SM-1-1-ECA	Ibid.	**MPI-ESM1-2-LR**	Ibid.
EC-Earth3	European Centre for Medium Range Weather Forecast	**MRI-ESM2-0**	International Centre for Theoretical Physics (Italy)
EC-Earth3-Veg	Ibid.	NESM3	Nanjing University of Information Science and Technology
FGOALS-f3-L	Institute of Atmospheric Physics (China)	NorCPM1	Bjerknes Centre for Climate Research (Norway)
FIO-ESM-2-0	First Institute of Oceanography	**NorESM2-LM**	Ibid.
GFDL-CM4	Geophysical Fluid Dynamics Laboratory (U.S.A)	**NorESM2-MM**	Ibid.
GFDL-ESM4	Ibid.	Sam0-UNICON	Seoul National University
GISS-E2-1-G	NASA Goddard Institute for Space Studies (U.S.A.)	**UKESM1-0-LL**	U.K. Met. Office

Table S1: A list of models from the CMIP6 ensemble and their associated modelling institution. All models ran historical simulations, bolded models ran the SSP585 scenario